Irrigation Science
https://doi.org/10.1007/s00271-023-00887-2

ORIGINAL PAPER

Evaluating the performance of the TSEB model for sorghum evapotranspiration estimation using time series UAV imagery

Emre Tunca[1]

Received: 26 January 2023 / Accepted: 21 September 2023

Abstract

Evapotranspiration (ET) is a vital process involving the transfer of water from the Earth's surface to the atmosphere through soil evaporation and plant transpiration. Accurate estimation of ET is important for a variety of applications, including irrigation management and water resource planning. The two-source energy balance (TSEB) model is a commonly used method for estimating ET using remotely sensed data. This study used the TSEB model and high-resolution unmanned aerial vehicle (UAV) imagery to estimate sorghum ET under four different irrigation regimes over two growing seasons in 2020 and 2021. The study also validated net radiation (Rn) flux through hand-held radiometer measurements and compared the estimated ET with a soil water balance model. The study outcomes revealed that that the TSEB model capably estimated Rn values, aligning well with ground-based Rn measurements for all irrigation treatments (RMSE = 32.9–39.8 W m^{-2} and MAE = 28.1–35.2 W m^{-2}). However, the TSEB model demonstrated robust performance in estimating ET for fully irrigated conditions (S1), while its performance diminished with increasing water stress (S2, S3, and S4). The R_2, RMSE, and MAE values range from 0.64 to 0.06, 10.94 to 17.04 mm, and 7.09 to 11.43 mm, respectively, across the four irrigation treatments over a 10-day span. These findings not only suggest the potential of UAVs for ET mapping at high-resolution over large areas under various water stress conditions, but also highlight the need for further research on ET estimation under water stress conditions.

Introduction

Agriculture, the world's primary food source (Küçüktopcu et al. 2022), has been facing numerous challenges due to prolonged drought conditions caused by climate change. The unstable pattern of rainfall coupled with high air temperatures requires precise information on crop evapotranspiration (ET) for effective irrigation scheduling, water conservation, and crop yield optimization (Zou et al. 2021). The agricultural industry consumes approximately 70% of the global freshwater supply (Phasinam et al. 2022), making it crucial to enhance water productivity to mitigate the impacts of climate change (Aguirre-García et al. 2021). Efficient water management strategies in agriculture, such as crop stress monitoring, can contribute to water conservation and cost reduction, including electricity expenses for water pumping (Togneri et al. 2019; Cáceres et al. 2021; Abioye et al. 2022). To achieve these objectives, reliable ET information is required at both spatial and temporal scales (Deus et al. 2013).

Traditionally, crop ET has been estimated using micrometeorological methods such as Eddy Covariance (Nassar et al. 2022), Scintillometer (Moorhead et al. 2017), or Bowen Ratio (Todd et al. 2000), as well as soil water balance approaches using lysimeters (Asadi and Kamran 2022), or changes in soil moisture content measured gravimetrically (Cemek et al. 2020) or with neutron probes (Koksal et al. 2017). However, these techniques offer limited spatial and temporal coverage and may not provide accurate ET estimates at the field scale (Singh Ramesh et al. 2008; Teixeira et al. 2009; Liaqat and Choi 2015). Moreover, direct measurement of ET over large areas is challenging. With the advent of remote sensing technology, several models have been proposed to estimate ET in various agricultural contexts, including horticulture (Tunca et al. 2022), field crops (Mokhtari et al. 2019; French et al. 2020), orchards (Nassar et al. 2021), and agro-ecological zones (Carpintero et al. 2020).

Remote sensing-based ET estimation methods can be broadly classified into three categories: (I) empirical models, which are derived from direct observations and

✉ Emre Tunca
emretunca@duzce.edu.tr

[1] Agriculture Faculty, Biosystem Engineering, Düzce University, Düzce, Turkey

Published online: 19 October 2023

measurements and often involve statistical relationships between observed ET and other measurable variables such as vegetation indices, meteorological data, or soil moisture content, (II) the relationship between remotely sensed surface temperatures and vegetation indices, and (III) surface energy balance models (Li et al. 2017; Knipper et al. 2019; Khosa et al. 2019). Empirical models depend on the quality of training data and may not be suitable for scaling to other regions (Li et al. 2021). The relationship between surface temperature and vegetation indices is based on the selection of dry and wet conditions in the regional ET, but it may be challenging to identify theoretical wet conditions in arid or semi-arid regions, which can impact the accuracy of ET estimates (Tang et al. 2010; Vinukollu et al. 2011). Surface energy balance models simulate the physical process of ET, with the latent heat flux (LE) calculated as a residual of the surface energy balance equation (Feng et al. 2020). Surface energy balance models, specifically two-source models, have demonstrated superior accuracy in estimating ET compared to alternative approaches. However, it is essential to note that the level of accuracy may differ across various SEBs. Hence, specific SEB models with lower precision may produce comparatively less accurate results than specific empirical models (Li et al. 2021).

Surface energy balance models can be divided into two categories: (1) one-source and (2) two-source models. One-source models evaluate the energy budget of soil and vegetation as a single component. In contrast, two-source models evaluate the energy budget of soil and vegetation separately (Taheri et al. 2022). Examples of one-source models include Mapping Evapotranspiration at High Resolution with Internalized Calibration (METRIC) (Allen et al. 2007), Surface Energy Balance Algorithm for Land (SEBAL) (Bastiaanssen et al. 1998), and Operational Simplified Surface Energy Balance (SSEBop) (Senay et al. 2007, 2013). Examples of two-source models include the Two Source Energy Balance (TSEB) (Norman et al. 1995), Atmosphere–Land Exchange Inverse model (ALEXI) (Mecikalski et al. 1999), and Dual Temperature Difference (DTD) (Norman et al. 2000). Two-source models provide a more physically accurate description of water and energy fluxes than one-source models (Burchard-Levine et al. 2021). They are, therefore, considered one of the most accurate techniques for estimating ET from remote sensing data (Li et al. 2021). In a study comparing the performance of METRIC, TSEB, and the Trapezoid Interpolation Model (TIM) during the Soil Moisture Atmosphere Coupling Experiment (SMACEX), Choi et al. (2009) found that TSEB outperformed TIM and METRIC. Previous research has also demonstrated a strong and consistent

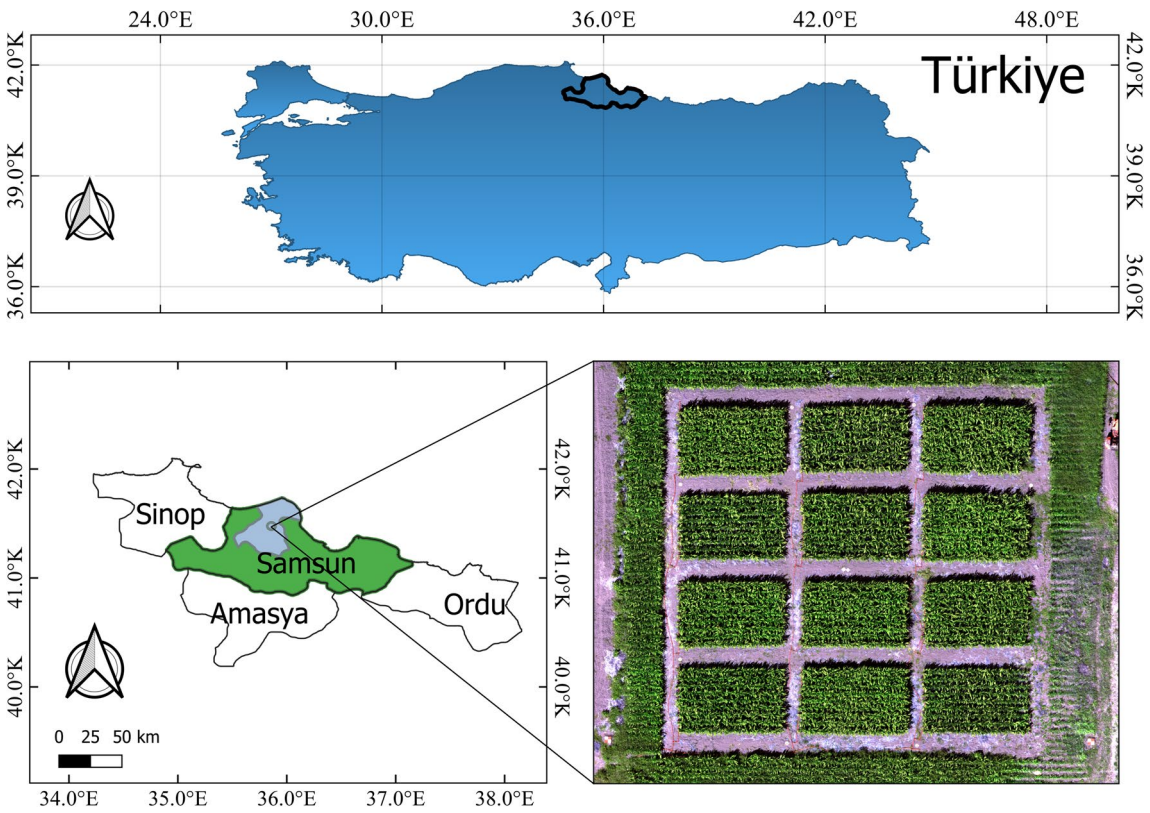

Fig. 1 Site overview of the study area

relationship between measured and estimated ET using TSEB models in a variety of crops, including cotton (Kustas and Norman 1999; Song et al. 2016), bell pepper (Tunca et al. 2022), vineyard (Gao et al. 2021), natural ecosystem (Nassar et al. 2022), wheat (Sánchez et al. 2015), sunflower (Sánchez et al. 2014) and maize (Sánchez et al. 2008). However, much of the literature on ET estimation using the TSEB model has focused on specific seasons or dates during the crop growing period and has primarily been conducted for fully irrigated crops, leaving the impact of time series data and multiple water stress conditions on ET estimation using the TSEB model largely unexplored.

This study aimed to evaluate the performance of the TSEB model in estimating ET using a time series of multispectral and thermal UAV images of a sorghum field irrigated under different water regimes during the 2020 and 2021 growing seasons. The net radiation (Rn) fluxes modeled using the TSEB model were validated using ground measurements, and the estimated ET products produced by the TSEB model were compared to those obtained using a soil–water balance approach.

Materials and methods

Study area

The experiment was conducted over two sorghum cropping years, 2020 and 2021, in a 0.1 ha research field located in Samsun, Turkey (41° 36′ 10.81″ N, 33° 55′ 13.57″ E, 16 m above sea level) (Fig. 1). The region is characterized by a sub-humid climate. A nearby meteorological station of the Turkish State Meteorological Service in Bafra/Samsun, situated approximately 150 m from the study area (41° 36′ 10.90″ N, 35° 55′ 13.56″ E and 16 m above sea level), recorded average annual daily air temperature of 14.6 °C and total precipitation of 717.9 mm per year from 1991 to 2020. The precipitation was distributed as follows: 29.43% in winter, 24.01% in spring, 16.49% in summer and 30.06% in autumn. The station is equipped with standard meteorological instruments that are regularly maintained and calibrated. The soil profile of the study area is predominantly clayey texture in the 0–90 cm layer, with 36% silt and 45% clay. From 90 to 120 cm, the soil profile displayed a texture characterized as clayey loam, consisting of 33% silt and 36% clay constituents (Köksal et al. 2011).

Field experimental design

The experiment utilized a drip irrigation system, comprising a control unit with a water pump, a fertilizer tank, and three filters: a vortex separator, a sand-media filter, and a screen filter. These filters were selected in accordance with the water quality and the requirements of the emitters. A dedicated valve and pressure meter controlled the irrigation provided to each experimental plot. Each crop row was irrigated using a single drip line, with drippers placed at 30 cm intervals and delivering a flow rate of 2 L per hour. The system maintained a pressure of 1.0 bar throughout the experiment. Prior to the experiment, a field test was conducted to collect data on system discharge, the wetting area diameter from the drippers, and the irrigation depth. This data was then used to determination of the irrigation duration for each experimental plot. Further details can be found in Köksal et al. (2017). The sorghum experiment followed a randomized block design with four irrigation treatments (0% (S4), 40% (S3), 70% (S2), and 100% (S1) of full irrigation) and three replications. S1 represented the full amount of irrigation required to satisfy the water needs of the sorghum crops throughout the growing season. Irrigation was applied when the soil moisture level decreased to 40% of the available soil water content and was replenished to field capacity, with 16 applications in 2020 and 10 in 2021. In contrast, rain-fed plots received irrigation only during the initial period (13 mm in 2020 and 25 mm in 2021), with no additional irrigation in either year. Soil water content was monitored using a neutron moisture meter (Model 503 DR, Campbell Pacific Nuclear, Martinez, CA). This device measured soil moisture at 30 cm intervals, down to a depth of 120 cm. In the center of each plot, a pair of access tubes were installed. One was placed approximately 10 cm away from the crop rows to effectively monitor the soil moisture variation within the crop root zone region. The second one was positioned between the crop row. The neutron moisture meter was calibrated at the beginning of the experiment, following the procedure outlined by Köksal et al. (2011). The irrigation was scheduled based on these soil water measurements.

The experimental plots were designed with dimensions of 10 m in length and 6.3 m in width, with 2.1 m alleys separating them. The sorghum variety "*Öğretmenoğlu*" was selected due to its widespread use in the region. The seeds were sown on May 15, 2020, and May 20, 2021, arranged in rows with a spacing of 0.7 m between rows and 0.05 m between plants. Based on the soil analysis results, fertilizers were applied at the rates of 64 kg ha^{-1} of N, 192 kg ha^{-1} of P_2O_5, and 64 kg ha^{-1} of K_2O. The sorghum grains were harvested on September 23, 2020, and September 27, 2021. The experiment followed standard cultivation practices for the region to minimize the influence of pests and diseases on crop performance.

Measuring of sorghum evapotranspiration

This study utilized the soil water balance method as the primary approach to validate the estimated ET for each plot.

The soil water content was monitored using a neutron probe prior to each irrigation event and on selected dates between irrigations. In situ, sorghum ET values were calculated for each treatment to maintain soil moisture levels between field capacity and readily available water (Eq. 1)

$$\mathrm{ET} = I + P - \mathrm{RO} - \mathrm{DP} + \mathrm{CR} \pm \Delta\mathrm{SF} \pm \Delta\mathrm{SW} \quad (1)$$

where I represents the amount of irrigation in mm; P is the precipitation in mm; RO is runoff (mm) which was ignored due to flat plot area and dense planting; DP is the deep percolation (mm) which was assumed to be zero due to controlled irrigation; CR is the capillary rise in mm; ΔSW is the changing soil water storage in mm.

Reference evapotranspiration ($\mathrm{ET_o}$) was calculated using the FAO Penman–Monteith equation to represent the atmosphere's evaporation demand (Eq. 2):

$$\mathrm{ET}_o = \frac{0.408\Delta\left(R_n - G\right) + \gamma\frac{900}{T+273}U_2(e_s - e_a)}{\Delta + \gamma(1 + 0.34U_2)} \quad (2)$$

where R_n is the net radiation (MJ m^{-2} day^{-1}); G is soil heat flux (MJ m^{-2} day^{-1}); T is mean air temperature (daily) at 2 m height (°C); U_2 is the wind speed at 2 m height (m s^{-1}); e_a and e_s are actual and saturated vapor pressure (kPa); Δ is the slope of the vapor pressure curve (kPa $°C^{-1}$), and γ is the psychrometric constant (kPa $°C^{-1}$).

Remote sensing and image processing

High-resolution multispectral and thermal images were captured using the DJI Matrice 300 RTK unmanned aerial vehicle (UAV) system (DJI Technology Co., China), equipped with a Micasense Altum sensor (Micasense, Seattle, Washington). The Altum camera features five high-resolution multispectral bands (blue, green, red, red edge, and near-infrared) in the VIS–NIR spectral range at 475, 560, 668, 717, and 840 nm, respectively, along with a longwave thermal sensor. The Altum sensor includes a Downward Light Sensor (DLS2) for calibrating multispectral images under various lighting conditions. The thermal sensor recalibrated itself every 5 min or following a 2 K temperature change. Each UAV flight followed a predefined flight plan, controlled automatically using DJI Pilot software. The UAV was flown at an altitude of 40 m above the ground to capture images with over 85% forward and side overlap. Each flight resulted in approximately 360 images, each with a footprint of 35 m × 26 m and a spatial resolution of 1.7 cm.

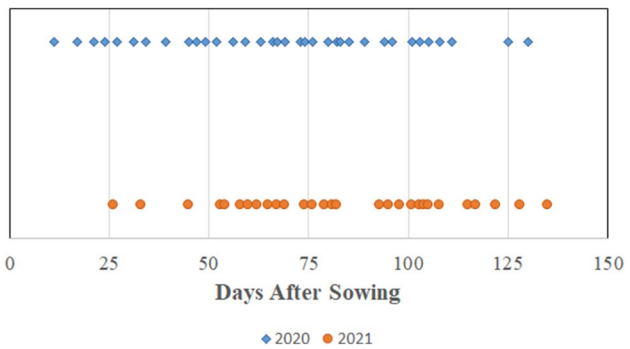

Fig. 2 Dates of UAS image acquisition

During the sorghum growing period, 37 UAV flights were conducted in 2020 and 31 flights in 2021, with the dates of the UAV image acquisitions shown in Fig. 2. All UAV flight missions were carried out under cloud-free conditions to prevent errors caused by clouds.

The high-resolution UAV images were captured between 12:30 PM and 1:30 PM local time. Before and after each UAV flight mission, images of the calibration panel were taken to convert the raw multispectral images into reflectance images.

The calibration of the multispectral images began with the conversion of raw pixel values from the calibration panel image into radiance units. Subsequently, the mean radiance value was computed for the pixels located within the reflectance panel area of the image. The transfer function, which converts radiance into reflectance for each spectral band, was then determined based on Eq. 3.

$$F_i = \frac{\rho_i}{\mathrm{avg}(L_i)} \quad (3)$$

F_i denotes the reflectance calibration factor, ρ_i signifies the reflectance value provided by the manufacturer, L_i represents the radiance for the reflectance panel pixels for band i.

The radiance, L, is calculated using the equation Eq. 4.

$$L = V(x,y) \times \frac{a_1}{g} \times \frac{p - p_{BL}}{t_e + a_2 y - a_3 t_e y} \quad (4)$$

where p is the normalized raw pixel value, p_{BL} is the normalized black level value, a_1, a_2 and a_3 are the radiometric calibration coefficients, $V(x, y)$ is the vignette polynomial function for pixel location (x, y), t_e is the image exposure time, and g is the sensor gain setting.

Subsequently, a vignette correction is executed to rectify the decrease in light sensitivity in pixels further from the image center. This is achieved using a 3-degree bivariate polynomial as per Eq. 5.

$$V(x,y) = \exp\left(\mathrm{sum}_{ij} c_{ij} x^i y^j\right). \quad (5)$$

To compensate for vignetting in the image, each pixel value is divided by the corresponding vignetting factor, as per the equation:

$$I'_{ij} = \frac{I_{ij}}{\exp(\text{sum}_{ij} c_{ij} x^i y^j)} \quad (6)$$

The variables x and y are calculated as:

$$x = 2 \times \frac{i + 0.5}{w - 1} \quad (7)$$

$$y = 2 \times \frac{j + 0.5}{h - 1} \quad (8)$$

where i and j are column and row pixel coordinates, w and h are image width and height in pixels, I_{ij} is the pixel intensity in the original image with vignetting, and I'_{ij} is the pixel intensity in the corrected image without vignetting. All the procedures above were conducted utilizing Agisoft Metashape, a photogrammetric processing software developed by Agisoft LLC, based in St Petersburg, Russia.

Sorghum canopy temperatures were measured using a handheld thermal imager (Testo, 875i) to facilitate comparison and calibration of the Micasense Altum's thermal band. The handheld thermal imager has a high-quality 32° × 23° lens and measurement accuracy of ± 2 °C.

The empirical line method, which is based on the linear relationship between the at-sensor radiometric temperature and corresponding surface temperature, was used to calibrate the Micasense Altum thermal band. The sensor's response range spans from 8 to 14 µm. Temperature measurements were conducted at solar noon under clear-sky conditions. The measurements were taken in four cardinal directions, namely east, west, north, and south, with three replications each and at an approximate height of 1 m above the canopy. The canopy temperatures for the plot were then calculated by averaging all the measurements.

Five different ground control points (GCPs) were positioned around the experimental plots and remained fixed throughout the sorghum growing period. Their locations were recorded with a hand-held GPS device (Geo7x, Trimble GeoExplorer, USA). These GCPs were utilized for geometric correction and aligning images acquired at different dates.

Rn is the primary driving force for the surface energy balance process and must be accurately estimated to obtain precise LE values, which are calculated as a residual of the surface energy balance equation.

To assess the accuracy of Rn estimates using the TSEB model, the estimated Rn values were compared with measurements taken using a CNR2 net radiometer (Kipp and Zonen, Delf, The Netherlands). Rn values for each experimental plot were measured 1 m above the crop canopy, considering the crops' growth. Rn was measured on four plants per plot, and the measurements were averaged to a single Rn value to represent the status of the experimental plot.

Determination of leaf area index

On the same day as the high-resolution UAV images acquisition, the in-situ leaf area index (LAI) was measured using a destructive method. For these measurements, three sorghum plants in each experimental plot were sampled at each sampling location. The leaves were detached, affixed to a sheet of white paper, and then scanned and scaled. The total area of the sorghum leaves was calculated to determine the LAI using Eq. 9. The average of the measurement results was taken as the LAI value for the experimental plot.

$$\text{LAI} = \frac{\text{Sorghum leaf area}}{\text{Row spacing} \times \text{crop distance}} \quad (9)$$

The LAI maps, which were used as input data for the TSEB model, were generated from an empirical regression of the multiplication of the Normalized Difference Vegetation Index (NDVI) and crop height (H_C) (NDVI x H_C) with the measured LAI obtained through a destructive in-situ method.

TSEB model

The two-source energy balance Model (TSEB) was initially developed by Norman et al. (1995) to separate turbulent fluxes between soil and canopy layers, thereby independently estimating evaporation and transpiration. The TSEB model was then updated by Kustas and Norman (1999) through improvements to the equations for soil surface resistance and partitioning of net radiation between the canopy and soil. A comprehensive explanation of the TSEB has been published by Norman et al. (1995), Guzinski et al. (2014) and Tunca et al. (2022), and here we provide a brief summary. In this study, the TSEB-PT version was used to estimate sorghum ET.

The TSEB-PT model assumes that the contribution of soil and vegetation to surface temperature can be separated based on canopy fractional cover (F_C). The model requires inputs such as H_C, LAI, radiometric surface temperature (T_s), F_C, and the ratio of canopy width to crop height ($W_C H_C^{-1}$). Additionally, the model requires meteorological data at the time of the UAV flight, including solar radiation (W m^{-2}), air temperature (K), vapor pressure (mBa), and wind speed (m s^{-1}).

In the TSEB model, net radiation R_n is partitioned into soil and vegetation sources using the following equations:

$$R_n = Rn_s + Rn_c \quad (10)$$

$$Rn_s = H_s + LE_s + G \quad (11)$$

$$Rn_c = H_c + LE_c \quad (12)$$

where R_n is the total net radiation (W m^{-2}); R_{ns} and R_{nc} are net radiation flux of soil and canopy, respectively (W m^{-2}).

G is estimated as a function of R_{ns} and is assumed to be 35% of R_{ns} (Norman et al. 1995).

$$G = c_G \times Rn_s \tag{13}$$

Sensible heat flux and sensible heat flux of soil (H_s) and canopy (H_c) are estimated as:

$$H_s = \rho C_p \frac{T_s - T_{AC}}{r_s} \tag{14}$$

$$H_C = \rho C_p \frac{T_C - T_{AC}}{r_x} \tag{15}$$

$$H = \rho C_p \frac{T_{AC} - T_A}{r_A} \tag{16}$$

where ρ is the air density (kg cm^{-3}); C_p is the heat capacity of the air (J Kg^{-1} K^{-1}) T_s, is soil temperature; T_c is canopy temperature; T_{AC} is the air temperature within the canopy boundary layer (K); T_A is the air temperature (K); r_A is the aerodynamic resistance (s m^{-1}); r_x is the resistance near the canopy layer (s m^{-1}) and r_s is the resistance above the soil surface layer (s m^{-1}). r_x and r_s calculations can be found in Norman et al. (1995). r_A can be calculated using solar radiation, air temperature, and wind speed. The formulations of Rn_s and Rn_c were given in Kustas and Norman (1999). LE_c was estimated by Priestley-Taylor method, as given in Eq. 18, while LE_s is considered as the residual of the energy balance equation.

$$\mathrm{LE} = \mathrm{LE}_c + \mathrm{LE}_s \tag{17}$$

$$\mathrm{LE}_c = \alpha_{PT} F_c \frac{\Delta}{\Delta + \gamma} \mathrm{Rn}_c \tag{18}$$

In Eq. 18, α_{PT} is the Priestley–Taylor coefficient. According to Norman et al. (1995), the initial value of α_{PT} is set to 1.26. F_c was calculated by the proportion of sorghum crops and bare soil within each spatial domain based on a binary classification of the high-resolution NDVI images. This study used the pyTSEB package (https://github.com/hectornieto/pyTSEB) to implement the TSEB-PT model. Standard input values (spectral properties, surface properties, resistance terms, etc.) were utilized provided by the PyTSEB.

The solar radiation method was used to extrapolate instantaneous LE to daily ET. This technique was established by Jackson et al. (1983) and assumes that ET is strongly correlated with Rs. Several studies, including Wandera et al. (2017), Tunca et al. (2022) and Nassar et al. (2021) have reported that the extrapolation of the incoming solar radiation has been relatively effective when applied to crops for estimating daily ET (Eq. 19).

$$\mathrm{ET}_d = \left(\frac{\mathrm{LE}}{R_s}\right)\left(\frac{c}{\rho_w \lambda}\right) R_{s_{24}} \tag{19}$$

In this equation, ET_d represents the total daily ET (mm day^{-1}), LE stands for the latent heat flux (W m^{-2}), Rs refers to the instantaneous incoming solar radiation (W m^{-2}), and $R_{s_{24}}$ denotes the daily incoming solar radiation (MJ/m^2/day). The symbol ρ_w is used to symbolize the density of water (kg m^{-3}), while λ is the latent heat of vaporization for water (MJ kg^{-1}). The numeral c represents the value of 1000, which is used to convert measurements from meters to millimeters.

The estimated ET values were interpolated between two consecutive UAV flight dates to derive daily ET values. This process began by dividing the estimated daily ET by the ETo for each flight date. These values were linearly interpolated for each day that fell between two consecutive UAV missions. Finally, the interpolated values were multiplied by the ETo of the corresponding day. This comprehensive process yielded a unique set of estimated daily ET values, providing a detailed understanding of ET throughout the study period.

Statistical analysis

The coefficient of determination (R^2), root mean square error (RMSE), and mean absolute error (MAE) were calculated to determine the robustness and precision of the TSEB model to estimate daily and seasonal ET. A higher R^2 value shows a better model fit, while a smaller RMSE and MAE value shows more accurate estimates (Eqs. 20–22).

$$R^2 = 1 - \frac{\sum_{i=1}^{n}(M_i - E_i)^2}{\sum_{i=1}^{n}(M_i - \underline{M}_1)^2} \tag{20}$$

$$\mathrm{RMSE} = \sqrt{\frac{\sum_{i=1}^{n}(M_i - E_i)^2}{n}} \tag{21}$$

$$\mathrm{MAE} = \frac{1}{n}\sum_{i=1}^{n}\left|M_i - E_i\right| \tag{22}$$

where M_i is the measured value, E_i is the estimated value; $\underline{M}_1$ is the average of measured values and n indicates the number of measurements.

Table 1 2020 and 2021 and long-term meteorological data for Bafra/Samsun

		May	June	July	August	September
Air temperature (ºC)	2020	16.2	21.5	24.1	22.6	21.9
	2021	17.0	20.2	24.9	23.9	18.5
	Long-term	15.1	19.9	22.9	23.6	20.3
Wind speed (U_2)	2020	2.58	2.41	2.19	2.37	1.96
	2021	2.63	1.89	2.65	2.13	1.95
	Long-term	1.26	1.44	1.72	1.71	1.50
Solar radiation (MJ m^{-2} d^{-1})	2020	24.3	26.6	26.4	25.6	18.3
	2021	24.0	23.7	27.2	21.6	14.9
	Long-term	20.1	23.3	23.2	20.5	15.3
Rainfall (mm)	2020	73.9	7.5	8.4	36.4	0.4
	2021	67.8	46.0	7.6	59.0	108.2
	Long-term	48.8	45.8	35.1	37.5	53.6
ETo (mm)	2020	138.1	161.9	173.2	167.5	117.5
	2021	147.0	143.8	186.0	143.4	92.0
	Long-term	103.4	129.8	142.7	125.1	82.2

Results and discussion

Meteorology

Table 1 presents the meteorological parameters for each month of the two consecutive sorghum growing seasons. The region's long-term average total rainfall over the past 30 years (1991–2020) from May to October is 220.8 mm. This is 94.2 mm more than the rainfall recorded during the 2020 sorghum growing period and 67.8 mm less than the 2021 season. The total rainfall for the two growing seasons of sorghum was 126.6 mm and 288.6 mm, respectively. The significant rainfall variation between the two years can be attributed to extreme precipitation events, specifically those that occurred from September 15 to September 26, 2021, which totaled 106.9 mm and significantly influenced the observed difference. The average daily air temperature ranged between 16.2 and 24.9 ºC during the study period. Meanwhile, the monthly average wind speed varied from 1.89 to 2.65 m s^{-1}. Additionally, solar radiation values were observed to fluctuate between 14.9 to 27.2 MJ $m^{-2}d^{-1}$.

The two growing seasons aligned with the long-term average meteorological data, with the exception of rainfall. The climatic conditions remained consistent throughout the two-year experiment, facilitating the evaluation of sorghum ET under various irrigation treatments while keeping agronomic and meteorological conditions stable.

Sorghum evapotranspiration

Figure 3 presents the ET values for each irrigation treatment across two sorghum growing seasons. To ensure uniform germination, a total of 13 and 25 mm of irrigation water were applied equally to all experimental treatments at the start of the growing seasons in 2020 and 2021, respectively. In both experimental years, treatment irrigation was initiated on June 15, 2020, and June 12, 2021, respectively, and terminated on September 25, 2020, and September 22, 2021. The total amount of irrigation applied across the range of treatments ranged from 13.0 to 701.4 mm in 2020 and 25.0 to 423.0 mm in 2021. Notably, the climatic conditions, as reflected by the seasonal ETo, differed in the two years, with values of 668.78 mm in 2020 and 608 mm in 2021. As the crops matured and the evaporative demand increased, the ET increased rapidly. The highest ET values were observed from early July to mid-August, which coincided with the maximum ground cover values (Fig. 4) and decreased towards the end of the growing season as the evaporative demand diminished.

During the sorghum growing period, the highest ET values were observed in the S1 treatment. As expected, the daily ET values were lower in the S4 treatment over both years. The seasonal sorghum ET values increased with the increasing amount of irrigation water. The seasonal ET values varied from 237.7 to 753.9 mm in the first year and 239.0–637.6 mm in the second year. The 18.2% higher seasonal ET value in 2020 is likely due to the 10.6% higher evaporative demand in that year compared to 2021.

Previous research has also investigated the crop ET rates of sorghum. For example, Garofalo and Rinaldi (2013) calculated sorghum ET values using the soil water balance method as 702 mm. Sakellariou-Makrantonaki et al. (2007) calculated the total water input to the root area as 777 mm. Abd El-Mageed et al. (2018) calculated the seasonal sorghum ET as 671 mm for full irrigation (100% FI), 570 mm for 85% FI, and 496 mm for 75% FI. The results of this study are generally consistent with these previous studies. However, the crop ET rate of sorghum was reported between 198

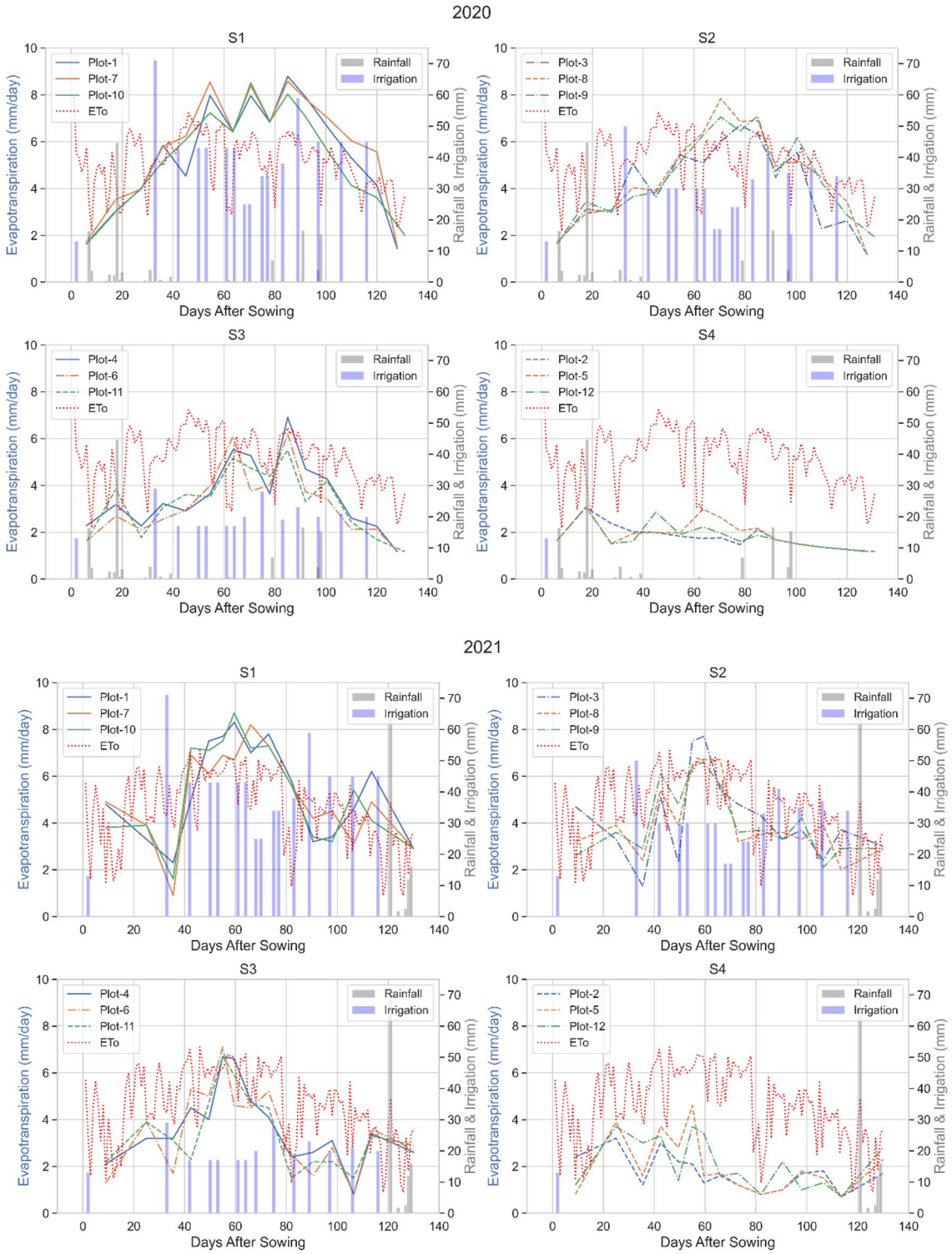

Fig. 3 Calculated ET values using the soil water balance method for each irrigation treatment, with reference to evapotranspiration (ETo), applied irrigation amounts, and precipitation events throughout the sorghum growing seasons of 2020 and 2021

and 553.6 mm by Aydinşakir et al. (2021), 400–428 mm by Lamm et al. (2010) and 240–500 mm by Hao et al. (2014). The ET values obtained in this study are slightly higher than those in the above literature. This discrepancy could be due to variations in climate, soil physical properties, sorghum varieties, and irrigation methods.

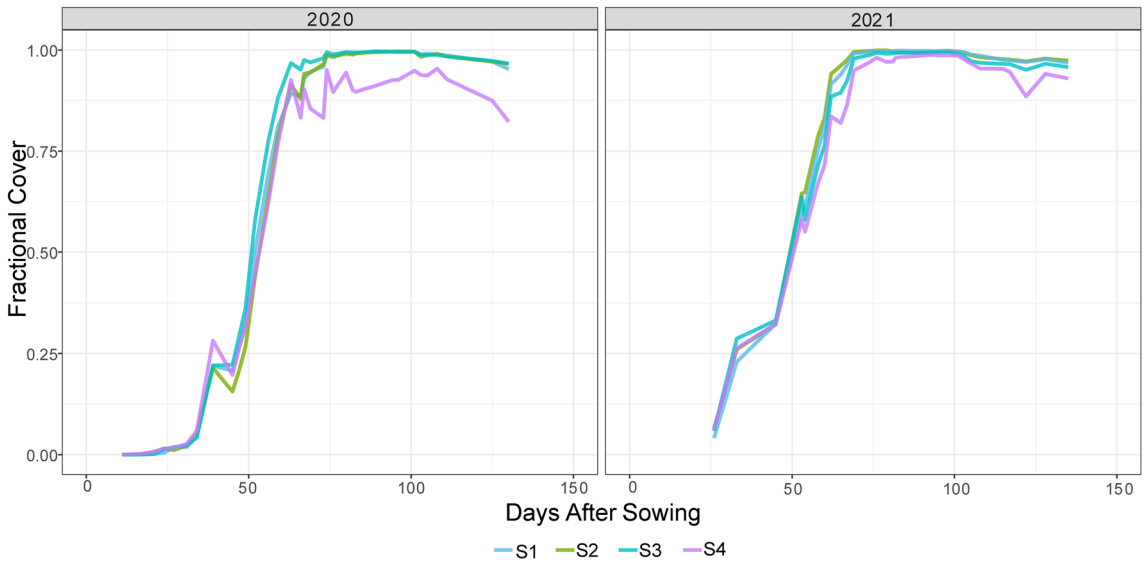

Fig. 4 Changes in sorghum fractional vegetation cover for 2020 and 2021

Sorghum leaf area index

Figure 5 shows the time series of in situ average LAI values among the treatments for each measurement date. In both experimental years, LAI was measured in 228 sorghum plants (120 in 2020 and 108 in 2021). Maximum LAI values were calculated at the mid-growing stage in both sorghum growing seasons (2020 and 2021). The S1 treatment demonstrated the highest LAI, with values of 11.0 and 11.2 measured at 102 and 97 days After Sowing (DAS) in 2020 and 2021, respectively. The LAI values obtained from this irrigation treatment differed significantly from the results obtained from other irrigation treatments ($p < 0.05$). Sorghum LAI values ranged from 0.3 to 11.0 in 2020 and 1.93–11.2 in 2021. In the first year, measured LAI values rose rapidly from DAS 41 to DAS 91, but then, decreased slightly from DAS 102 to DAS 132. The LAI values in 2021 increased rapidly during the development stage (between DAS 56 and 77), and the peak LAI (11.2) was reached at DAS 97. The LAI values of this study are consistent with those reported by Aydinşakir et al. (2021), who concluded that maximum LAI values varied between 9.0 and 16.1. In

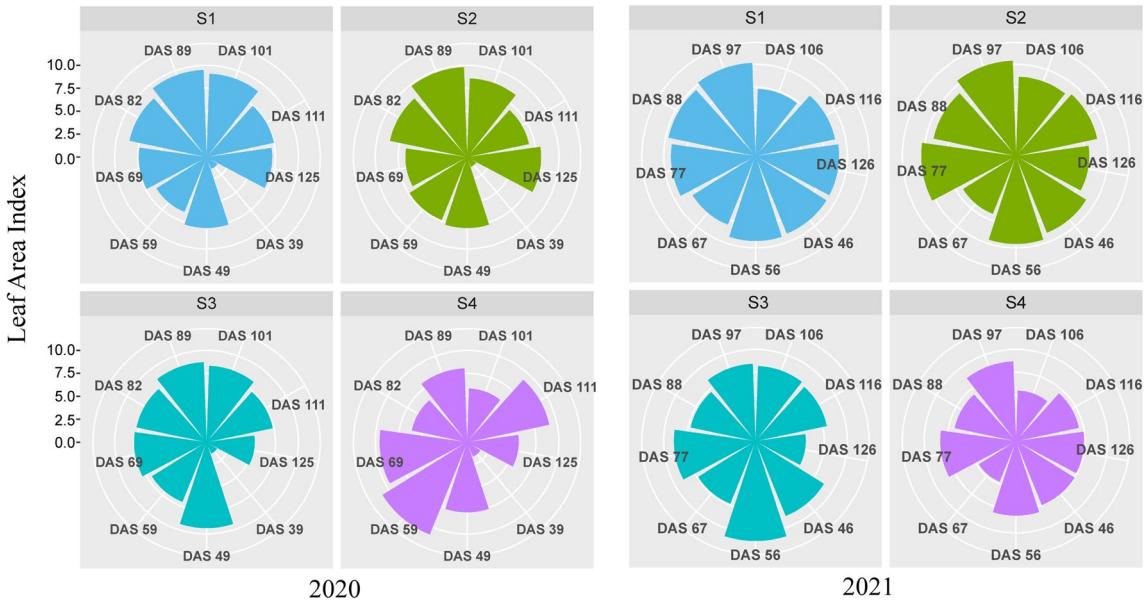

Fig. 5 In situ measured average LAI values for each irrigation treatment in 2020 and 2021

the experiment of GhassemiSahebi et al. (2020), the seasonal average LAI values ranged from 4.43 to 7.38. The maximum sorghum LAI value was calculated as 11.0 by Sánchez et al. (2011). Following the results of this study, previous studies have shown that LAI values decreased after a period of water stress. For example, Campi et al. (2016) indicated that LAI in fully-irrigated sorghum plants was 35% higher in comparison to water-stressed. The same results were found by Cosentino et al. (2012) and Aydınşakir et al. (2021).

Figure 6 provides the scatter diagram of the relationship between the estimated and measured sorghum LAI. Results indicated that estimated LAI had a good consistency with the in situ measured LAI, indicating an R^2, RMSE and MAE of 0.81, 1.17 and 0.81 m^{-2} m^{-2}, respectively. Estimated sorghum LAI values ranged from 1.9 to 10.68 m^{-2} m^{-2} in 2020 and from 2.1 to 10.5 m^{-2} m^{-2} in 2021. However, one drawback of the empirical models used in this study is that they strictly depend on the collection and quality of the ground data. Some errors could occur with in situ LAI measurements, which could affect the LAI estimation (Gano et al. 2021). On the other hand, remote sensing is a widely used technique to estimate LAI due to its fast and accurate LAI estimation. Previous research has already demonstrated the potential of using vegetation indexes calculated from remotely sensed data, such as the NDVI, to estimate sorghum LAI (Potgieter et al. 2017; Shafian et al. 2018). However, a saturation of NDVI at high LAI values has been reported by several researchers (Huang et al. 2015; Huete et al. 2002; Potgieter et al. 2017; Tunca et al. 2018). Also, this problem may partly be explained by Mutanga and Skidmore (2004), who concluded that other indices could be used rather than NDVI due to saturation after canopy closure. In this study, we developed a new approach to estimate sorghum LAI based on NDVI and H_c obtained from UAV images. Overall, the results of this study indicated that the generated LAI maps reasonably capture both spatial and temporal sorghum LAI variability within the study area and that these maps are reliable for use in ET mapping with the TSEB model.

Comparison of ground and UAV thermal image

Figure 7 compares thermal images captured from a UAV system and a hand-held ground thermal imager over two consecutive growing seasons. The results demonstrate a strong correlation between the temperature values obtained from the UAV system and those from the ground-based thermal imager across different irrigation treatments, with the scatter points in the graph closely aligned with the 1:1 line.

The most significant discrepancies between the UAV and ground-based thermal measurements were approximately 6 °C for both years. The highest and lowest temperatures measured with the UAV system were 46.4 °C (DAS 76) and 24.7 °C (DAS 28), respectively, while the highest and lowest temperatures measured with the ground thermal imager were 49.4 °C (DAS 76) and 24.2 °C (DAS 28), respectively. A significant correlation was observed between the two measurements, with a coefficient of determination (R^2) of 0.91 and RMSE and MAE values of 2.01 °C and 1.55 °C, respectively, which are consistent with the accuracy of the Micasense Altum camera. These findings are similar to previous studies (Awais et al. 2022; Malbéteau et al. 2018; Simpson et al. 2021; Song and Park 2020; Tunca et al. 2022). Several factors can influence the accuracy of UAV thermal temperatures, such as climatic conditions like wind, air temperature, and humidity, and environmental conditions like emissivity and the distance between the thermal camera and the target (Acorsi et al. 2020). Additionally, factors like UAV flight height, camera shooting angle, and vignetting can also impact thermal accuracy (Kelly et al. 2019).

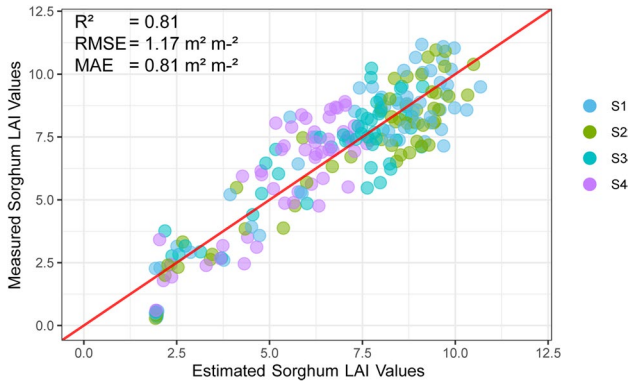

Fig. 6 Scatterplot of the sorghum LAI estimated values vs in-situ measured values

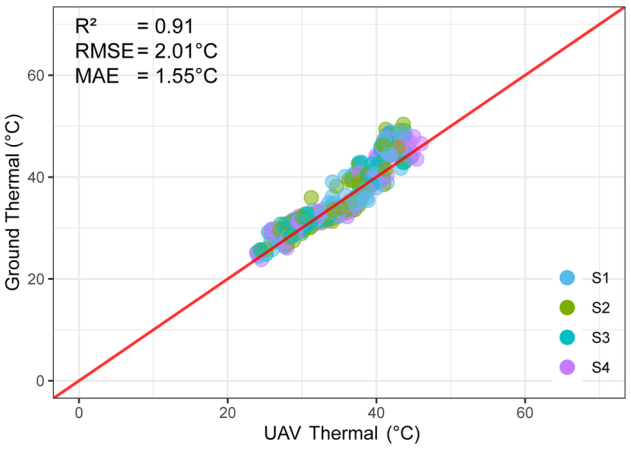

Fig. 7 Comparison of thermal images taken from UAV system and hand-held ground thermal imager

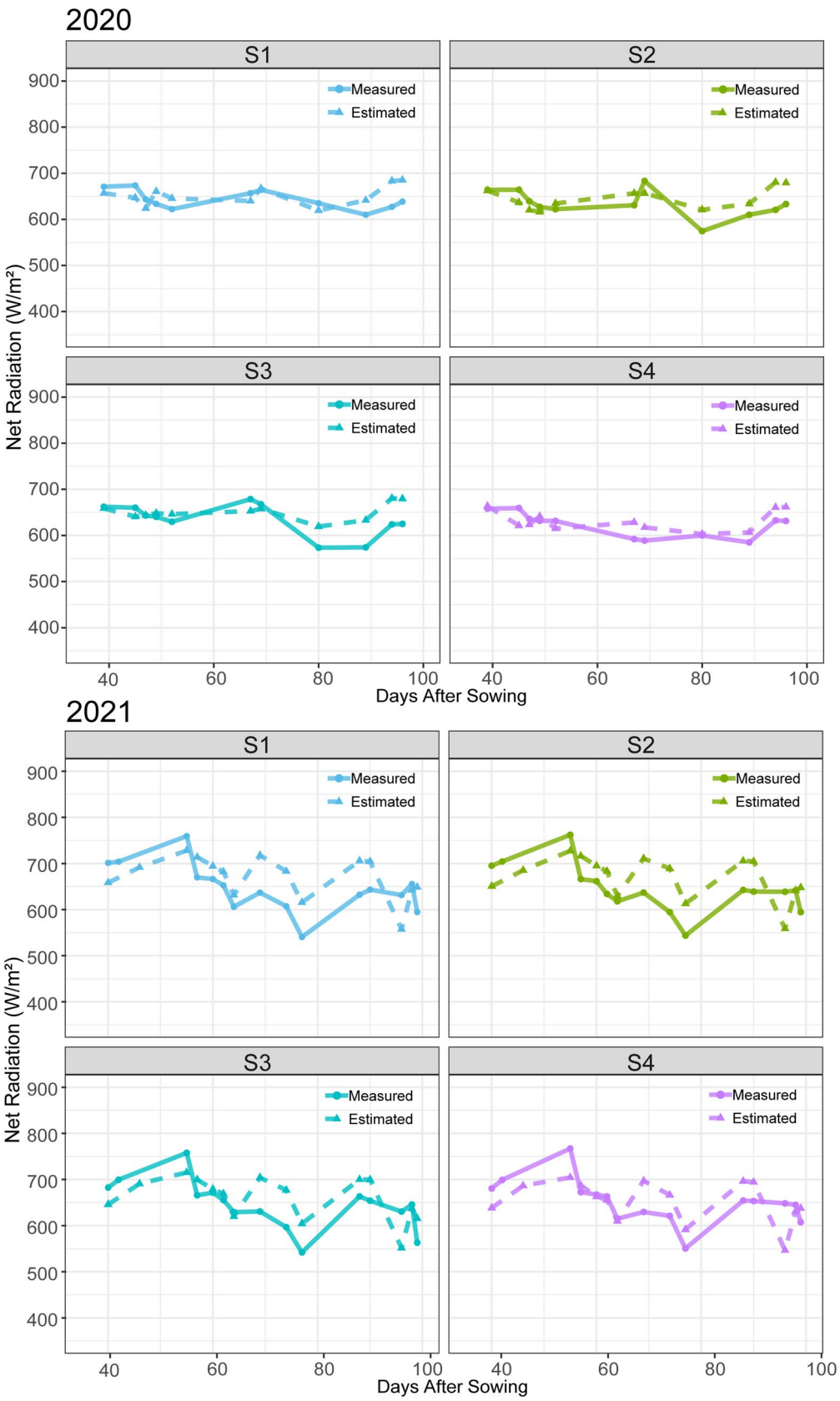

Fig. 8 Time series of average Rn estimates from the TSEB model against in situ measurements during the two sorghum growing periods

Table 2 Goodness-of-fit statics between the measured net radiation (W m^{-2}) and the estimated net radiation (W m^{-2}) using the TSEB model at different irrigation treatments

	R^2	RMSE (W m^{-2})	MAE (W m^{-2})
S1	0.56	39.6	35.2
S2	0.42	39.7	34.7
S3	0.49	39.8	33.7
S4	0.47	332.9	28.1

Table 3 Statistical analysis results from TSEB-PT model estimations ET vs. measured ET using neutron probe for ten days

	R^2	MAE (mm 10 day^{-1})	RMSE (mm 10 day^{-1})
S1	0.64	7.09	10.94
S2	0.30	8.58	12.71
S3	0.09	8.95	14.22
S4	0.06	11.43	17.04

Net radiation results

Figure 8 presents a time series comparison of average Rn estimates from the TSEB model and in situ measurements during the two sorghum growing periods. The highest recorded Rn values were observed in plots subjected to S1 irrigation treatments (685.1 W m^{-2} in 2020 and 728.2 W m^{-2} in 2021), while the lowest Rn value was noted in S4 irrigation plots (597.8 W m^{-2} in 2020 and 546.60 W m^{-2} in 2021). Similarly, the estimated maximum and minimum Rn values were found in S1 (715.9 W m^{-2} in 2020 and 767.2 W m^{-2} in 2021) and S4 (551.0 W m^{-2} in 2020 and 540.5 W m^{-2} in 2021) treatments, respectively. This could be attributed to the fact that S1 treatment plots have moist soil while S4 treatment plots have a dry soil surface. The differences could be related to the higher albedo values of dry soil (S4) and its higher surface temperature values, which cause a decrease in Rn values for S4 treatment plots. These findings are in line with previous research, such as Ben-Asher et al. (1978), who demonstrated that soil surfaces with higher moisture content exhibited greater Rn values than those that were only partially moistened. Furthermore, this study's results are consistent with the work of Kalita and Kanwar (1992), who found significant variations in the Rn values of corn at different soil moisture content levels. Köksal et al. (2018) found that Rn values did not differ among irrigation treatments. However, larger Rn values were obtained from fully irrigated plots..

In general, the estimated Rn values using the TSEB model captured well the measured Rn values for all experimental treatments during the two sorghum growing seasons (Table 2). These results are in agreement with previous research on TSEB-based Rn estimation, where calculated RMSE for estimated Rn ranged between 26 and 43 W m^{-2}

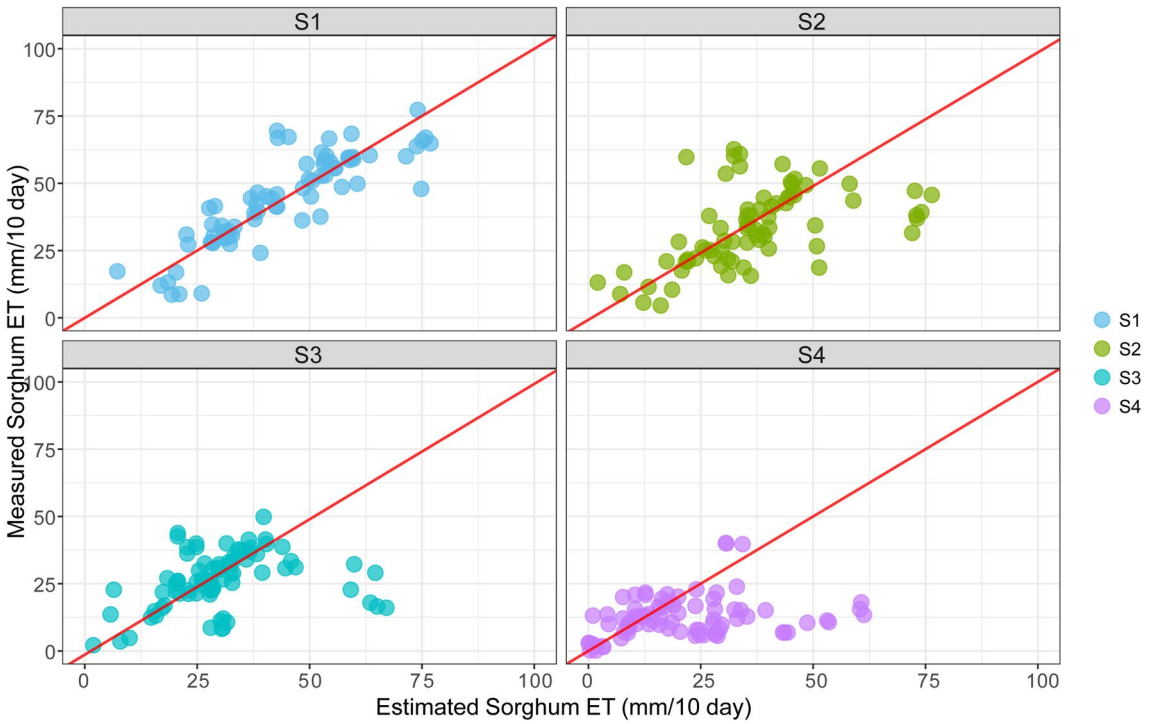

Fig. 9 Comparison of estimated sorghum ET by using the TSEB model and measured sorghum ET using the soil water balance approach

(Nassar et al. 2021), 30–50.1 W m^{-2} (Gan and Gao 2015), 10.90–58.95 W m^{-2} (Khan et al. 2021), 63 W m^{-2} with Sentinel 2 + 3 images and 103 W m^{-2} with Landsat 8 images (Jofre-Čekalović et al. 2022), and 44.2 W m^{-2} (Chávez et al. 2009). The slight difference between estimated and measured Rn values can be explained by errors in the estimation of Rn caused by TSEB model parameters, as well as dust and heating of the downward-facing pyrgeometer of the device. Another possible reason for the discrepancies is the difference in the field of view (FOV) between the net radiometer and Micasense Altum. The net radiometer used in this study had an FOV of 180° for the upper detector and 150° for the lower detector, while the Micasense Altum had an FOV of 48° × 37°. The wider FOV instrument receives proportionally more radiation from its environment than the narrow one (Micasense Altum), resulting in the Micasense Altum receiving radiation from a more homogeneous area than the hand-held net-radiometer device.

Sorghum TSEB results

Sorghum ET values, calculated using the soil water balance method were used as a reference for evaluating the ET output from the TSEB model. The estimated ET maps are provided as a time series in the Appendix. Since the neutron probe measurements were taken with a ten-day interval, the sorghum ET values were reported as mm 10 $days^{-1}$. However, it was not always possible to align UAV image acquisition with neutron probe measurements due to adverse weather conditions such as cloud cover or strong winds. The results of the TSEB-based ET values are not transferred from one day to another. Therefore, a fraction of the estimated ET (ET/ETo) was used for linear interpolation between sequential UAV missions to obtain ET values that coincided with two consecutive neutron probe measurement periods. While the soil water balance method for calculating crop ET is not an actual ET measurement method, it remains a popular approach for evaluating estimated ET for TSEB, as demonstrated in studies by (Liang et al. 2021; Sau et al. 2004; Tunca et al. 2022). Other researchers have used the Eddy Covariance system to validate TSEB-based estimated ET and surface energy balance components (Hoffmann et al. 2015; Nassar et al. 2021). However, the EC measurement technique was not suitable for our study plots due to their small size (6.3 m × 10 m), which is not compatible with the footprint of the EC tower.

Figure 9 presents a comparison of measured and estimated ET values for 10-day intervals. The corresponding R^2, MAE, and RMSE values are detailed in Table 3. The range of measured ET values was between 0.7 to 83.6 mm 10 day^{-1}, while the TSEB model estimated ET values between 0.3 and 75.5 mm 10 day^{-1}. The maximum and minimum measured and estimated ET values were observed in S1 and S4 treatments, respectively. The MAE and RMSE of measured and estimated ET varied between 7.09 (~0.70 mm day^{-1}) and 11.43 mm 10 day^{-1} (~1.14 mm day^{-1}) and 10.94 (~1.09 mm day^{-1}) to 17.04 mm 10 day^{-1} (~1.7 mm day^{-1}), respectively. Liang et al. (2021) assessed the TSEB model's performance against the ET derived from a neutron probe in a fully irrigated dry edible bean field, reporting RMSE values ranging from 3.3 to 9.7 mm $week^{-1}$. French et al. (2015) found a difference of 2 mm per day between the ET estimated with TSEB and the ET measured from the neutron probe. Similar results were reported in studies using the TSEB model for sorghum (Sánchez et al. 2011), cotton (Colaizzi et al. 2014) and sunflower and canola (Sánchez et al. 2014).

As depicted in Fig. 9, the estimated ET values for the S1 treatment exhibit a similar variation trend to the measured ET values. However, the results for the S4 treatment showed poor performance across two years. These discrepancies can be attributed to the increase in deficit irrigation from S1 to S4, which leads to an increase in water deficit in the root zone. The soil moisture deficiency, evident in the neutron probe measurements in the S4 treatments, was not accurately predicted by the TSEB model. Zhuang and Wu (2015) suggested that the α_{PT} parameter of 1.3 is appropriate for fully irrigated crops. However, when this parameter was applied to high-resolution UAV images covering unstressed (S1) and stressed (S2, S3, and S4) sorghum treatment plots, the TSEB model overestimated sorghum ET for stressed treatments. Guzinski et al. (2013) pointed out that TSEB is sensitive to the parameter and requires manual adjustment under stress conditions. However, this approach may be subjective as the stress level of vegetation is not always accurately discernible. Recent studies have indicated that the TSEB model can overestimate crop ET, particularly under high water stress and low vegetation cover conditions (Gonzalez-Dugo et al. 2009; Long and Singh 2012; Morillas et al. 2014; Bellvert et al. 2023). In this study, Rn is generally overestimated by TSEB. This overestimation could be attributed to the meteorological data used in this study. The overestimation of Rn subsequently leads to an overestimation of sorghum ET (Chen et al. 2022).

Another source of uncertainty in TSEB-based ET estimation is the presence of shadow pixels. Pixels containing shadows result in a lower surface temperature, which increases the measured ET compared to pixels containing only vegetation (Mokhtari et al. 2021).

The sensor used in this study also contributes to the discrepancy between estimated and measured ET values. The thermal images obtained through UAVs equipped with thermal cameras exhibit various sources of uncertainty, including the internal non-uniformity correction and temperature drift, as well as environmental factors such as air humidity and surface emissivity property (Aubrecht et al. 2016; Meier et al. 2011; Mesas-Carrascosa et al. 2018; Olbrycht

et al. 2012; Peng et al. 2023). The presence of uncertainties directly impacts the quality of the acquired UAV thermal images. These uncertainties directly impact the quality of the acquired UAV thermal images. Therefore, it is crucial to prioritize specific steps, such as updating the camera system and conducting radiometric calibration of the thermal data, to enhance the accuracy and reliability of the data collection process. Overall, while TSEB-based ET estimates can generally capture variability between the experimental treatments, the accuracy diminishes with increasing water stress.

Conclusion

This research utilized the TSEB model in conjunction with high-resolution UAV imagery to estimate Rn and ET values for sorghum. Estimated values were then compared with measured Rn obtained from a net radiometer and calculated ET derived from neutron probe measurements across two sorghum growing periods. The TSEB model yielded satisfactory estimates of Rn for each irrigation treatment, although the ET estimation error increased with a higher degree of water stress level. The RMSE and MAE between estimated and measured sorghum Rn ranged between 32.9 to 39.8 W m^{-2} and 28.1 to 35.2 W m^{-2}, respectively. The highest accuracy for sorghum ET estimation was obtained from S1 treatments ($R^2 = 0.64$, RMSE = 10.94 mm 10 day^{-1} (~ 1.09 mm day^{-1}), while the lowest accuracy was obtained from S4 treatments ($R^2 = 0.06$, RMSE = 17.04 mm 10 day^{-1} (~ 1.70 mm day^{-1}).

These results suggest that the TSEB model can effectively estimate ET under non-stressed conditions and can be employed for full-irrigation scheduling. However, to enhance the TSEB model's performance under water stress conditions, further research is required. Additionally, testing different TSEB models (TSEB-2T, TSEB-PM, and TSEB-DTD) across various crop types is recommended. Furthermore, future studies should incorporate different sensors to gain a more comprehensive understanding of their impact on ET estimation.

Appendix

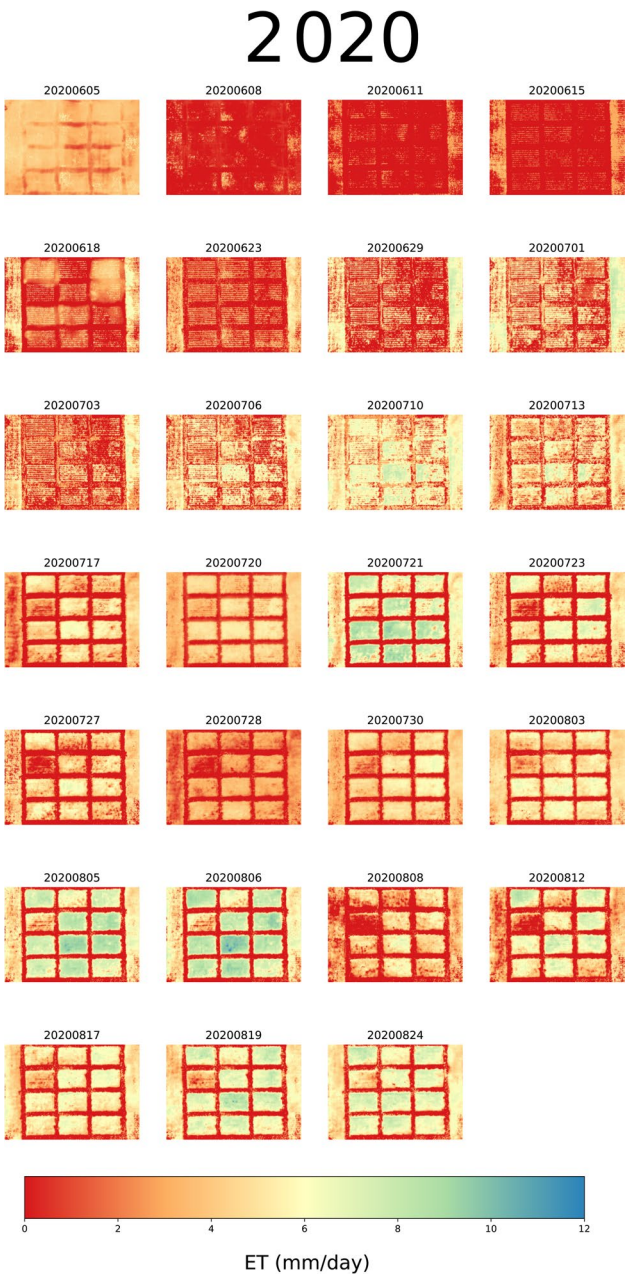

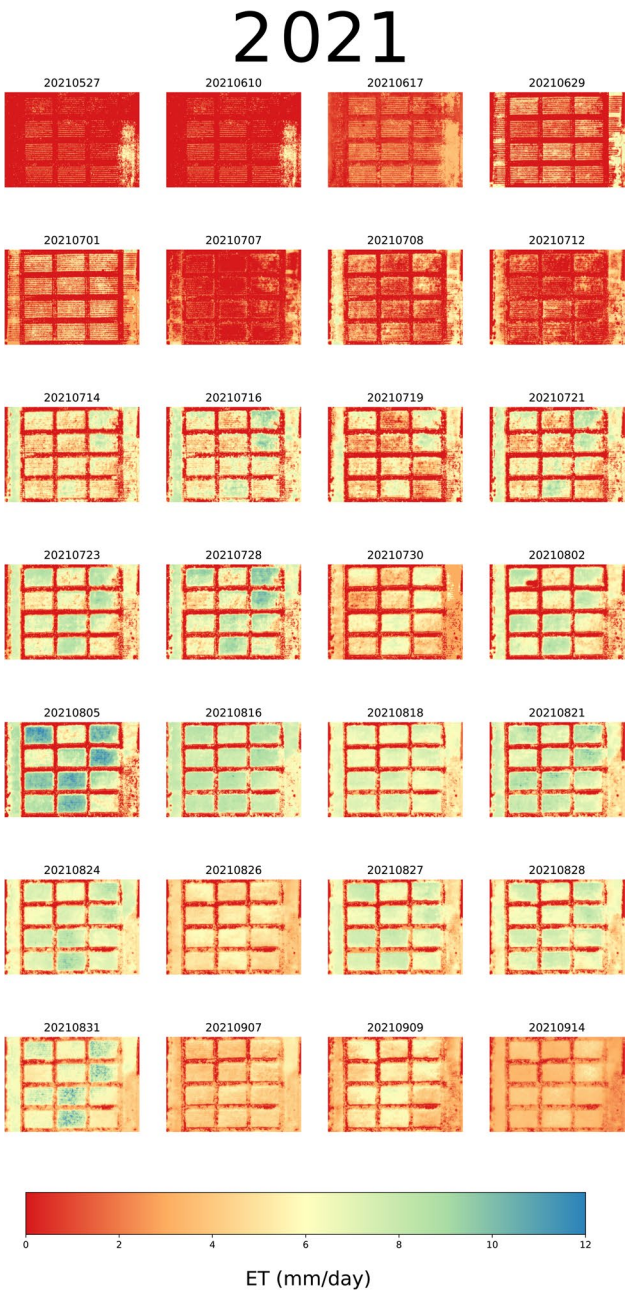

Acknowledgements This study was supported by the Scientific and Technical Research Council of Turkey (TUBITAK, Project Number: 118O831).

Author contributions The author conducted the study, drafted the manuscript, and analyzed the data. The figures and tables of the manuscript were made by the author.

Declarations

Conflict of interest The author declares that no conflicts of interest relevant to this study.

References

Abd El-Mageed TA, El- Samnoudi IM, Ibrahim AE-AM, Abd El Tawwab AR (2018) Compost and mulching modulates morphological, physiological responses and water use efficiency in sorghum (bicolor L. Moench) under low moisture regime. Agric Water Manag 208:431–439. https://doi.org/10.1016/j.agwat.2018.06.042

Abioye EA, Hensel O, Esau TJ et al (2022) Precision irrigation management using machine learning and digital farming solutions. AgriEngineering 4:70–103. https://doi.org/10.3390/agriengineering4010006

Acorsi MG, Gimenez LM, Martello M (2020) Assessing the performance of a low-cost thermal camera in proximal and aerial conditions. Remote Sens 12:3591. https://doi.org/10.3390/rs12213591

Aguirre-García S-D, Aranda-Barranco S, Nieto H et al (2021) Modelling actual evapotranspiration using a two source energy balance model with Sentinel imagery in herbaceous-free and herbaceous-cover Mediterranean olive orchards. Agric for Meteorol 311:108692. https://doi.org/10.1016/j.agrformet.2021.108692

Allen RG, Masahiro T, Ricardo T (2007) Satellite-based energy balance for mapping evapotranspiration with internalized calibration (METRIC)—Model. J Irrig Drain Eng 133:380–394. https://doi.org/10.1061/(ASCE)0733-9437(2007)133:4(380)

Asadi M, Kamran KV (2022) Comparison of SEBAL, METRIC, and ALARM algorithms for estimating actual evapotranspiration of wheat crop. Theor Appl Climatol 149:327–337. https://doi.org/10.1007/s00704-022-04026-3

Aubrecht DM, Helliker BR, Goulden ML et al (2016) Continuous, long-term, high-frequency thermal imaging of vegetation: Uncertainties and recommended best practices. Agric for Meteorol 228:315–326. https://doi.org/10.1016/j.agrformet.2016.07.017

Awais M, Li W, Hussain S et al (2022) Comparative evaluation of land surface temperature images from unmanned aerial vehicle and satellite observation for agricultural areas using in situ data. Collect FAO Agric 12:184. https://doi.org/10.3390/agriculture12020184

Aydinsakir K, Buyuktas D, Dinç N et al (2021) Yield and bioethanol productivity of sorghum under surface and subsurface drip irrigation. Agric Water Manag 243:106452. https://doi.org/10.1016/j.agwat.2020.106452

Bastiaanssen WGM, Menenti M, Feddes RA, Holtslag AAM (1998) A remote sensing surface energy balance algorithm for land (SEBAL). 1. Formulation. J Hydrol 212–213:198–212. https://doi.org/10.1016/S0022-1694(98)00253-4

Bellvert J, Pelechá A, Pamies-Sans M et al (2023) Assimilation of sentinel-2 biophysical variables into a digital twin for the automated irrigation scheduling of a vineyard. Water 15(14):2506. https://doi.org/10.3390/w15142506

Ben-Asher J, Fuchs M, Goldberg D (1978) Radiation and energy balance of sprinkler and trickle irrigated fields[1]. Agron J 70:415–417. https://doi.org/10.2134/agronj1978.00021962007000030012x

Burchard-Levine V, Nieto H, Riaño D et al (2021) The effect of pixel heterogeneity for remote sensing based retrievals of evapotranspiration in a semi-arid tree-grass ecosystem. Remote Sens Environ 260:112440. https://doi.org/10.1016/j.rse.2021.112440

Cáceres G, Millán P, Pereira M, Lozano D (2021) Smart farm irrigation: model predictive control for economic optimal irrigation in agriculture. Agronomy 11:1810. https://doi.org/10.3390/agronomy11091810

Campi P, Navarro A, Palumbo AD et al (2016) Energy of biomass sorghum irrigated with reclaimed wastewaters. Eur J Agron 76:176–185. https://doi.org/10.1016/j.eja.2016.01.015

Carpintero E, Andreu A, Gómez-Giráldez PJ et al (2020) Remote-sensing-based water balance for monitoring of evapotranspiration

and water stress of a Mediterranean Oak-Grass Savanna. Water 12:1418. https://doi.org/10.3390/w12051418

Cemek B, Ünlükara A, Kurunç A, Küçüktopcu E (2020) Leaf area modeling of bell pepper (*Capsicum annuum* L.) grown under different stress conditions by soft computing approaches. Comput Electron Agric 174:105514. https://doi.org/10.1016/j.compag.2020.105514

Chávez JL, Gowda PH, Howell TA et al (2009) Estimating hourly crop ET using a two-source energy balance model and multispectral airborne imagery. Irrig Sci 28:79–91. https://doi.org/10.1007/s00271-009-0177-9

Chen D, Zhuang Q, Zhang W et al (2022) Estimation of Landsat-like daily evapotranspiration for crop water consumption monitoring using TSEB model and data fusion. PLoS ONE 17(5):e0267811. https://doi.org/10.1371/journal.pone.0267811

Choi M, Kustas WP, Anderson MC et al (2009) An intercomparison of three remote sensing-based surface energy balance algorithms over a corn and soybean production region (Iowa, US) during SMACEX. Agric for Meteorol 149:2082–2097. https://doi.org/10.1016/j.agrformet.2009.07.002

Colaizzi PD, Agam N, Tolk JA et al (2014) Two-source energy balance model to calculate E, T, and ET: comparison of Priestley-Taylor and penman-Monteith formulations and two time scaling methods. Trans ASABE. https://doi.org/10.13031/trans.57.10423

Cosentino SL, Mantineo M, Testa G (2012) Water and nitrogen balance of sweet sorghum (*Sorghum bicolor* moench (L.)) cv. Keller under semi-arid conditions. Ind Crops Prod 36:329–342. https://doi.org/10.1016/j.indcrop.2011.10.028

de Teixeira AHC, Bastiaanssen WGM, Ahmad BMG (2009) Reviewing SEBAL input parameters for assessing evapotranspiration and water productivity for the Low-Middle São Francisco River basin, Brazil: part a: calibration and validation. Agric for Meteorol 149:462–476. https://doi.org/10.1016/j.agrformet.2008.09.016

Deus D, Gloaguen R, Krause P (2013) Water balance modeling in a semi-arid environment with limited in situ data using remote sensing in Lake Manyara, East African Rift, Tanzania. Remote Sens 5:1651–1680. https://doi.org/10.3390/rs5041651

Feng J, Wang W, Xu F, Sun S (2020) Estimating surface heat and water vapor fluxes by combining two-source energy balance model and back-propagation neural network. Sci Total Environ 729:138724. https://doi.org/10.1016/j.scitotenv.2020.138724

French AN, Hunsaker DJ, Thorp KR (2015) Remote sensing of evapotranspiration over cotton using the TSEB and METRIC energy balance models. Remote Sens Environ 158:281–294. https://doi.org/10.1016/j.rse.2014.11.003

French AN, Hunsaker DJ, Sanchez CA et al (2020) Satellite-based NDVI crop coefficients and evapotranspiration with eddy covariance validation for multiple durum wheat fields in the US Southwest. Agric Water Manag 239:106266. https://doi.org/10.1016/j.agwat.2020.106266

Gan G, Gao Y (2015) Estimating time series of land surface energy fluxes using optimized two source energy balance schemes: model formulation, calibration, and validation. Agric for Meteorol 208:62–75. https://doi.org/10.1016/j.agrformet.2015.04.007

Gano B, Dembele JSB, Ndour A et al (2021) Using UAV borne, multispectral imaging for the field phenotyping of shoot biomass, leaf area index and height of West African Sorghum varieties under two contrasted water conditions. Agronomy 11:850. https://doi.org/10.3390/agronomy11050850

Gao R, Torres-Rua A, Nassar A et al (2021) Evapotranspiration partitioning assessment using a machine-learning-based leaf area index and the two-source energy balance model with sUAV information. In: Autonomous Air and Ground Sensing Systems for Agricultural Optimization and Phenotyping VI. SPIE, pp 106–129

Garofalo P, Rinaldi M (2013) Water-use efficiency of irrigated biomass sorghum in a Mediterranean environment. Span J Agric Res 11:1153–1169. https://doi.org/10.5424/sjar/2013114-4147

GhassemiSahebi F, Mohammadrezapour O, Delbari M et al (2020) Effect of utilization of treated wastewater and seawater with Clinoptilolite-Zeolite on yield and yield components of sorghum. Agric Water Manag 234:106117. https://doi.org/10.1016/j.agwat.2020.106117

Gonzalez-Dugo MP, Neale CMU, Mateos L et al (2009) A comparison of operational remote sensing-based models for estimating crop evapotranspiration. Agric for Meteorol 149:1843–1853. https://doi.org/10.1016/j.agrformet.2009.06.012

Guzinski R, Anderson MC, Kustas WP et al (2013) Using a thermal-based two source energy balance model with time-differencing to estimate surface energy fluxes with day–night MODIS observations. Hydrol Earth Syst Sci 17:2809–2825. https://doi.org/10.5194/hess-17-2809-2013

Guzinski R, Nieto H, Jensen R, Mendiguren G (2014) Remotely sensed land-surface energy fluxes at sub-field scale in heterogeneous agricultural landscape and coniferous plantation. Biogeosciences 11:5021–5046. https://doi.org/10.5194/bg-11-5021-2014

Hao B, Xue Q, Bean BW et al (2014) Biomass production, water and nitrogen use efficiency in photoperiod-sensitive sorghum in the Texas High Plains. Biomass Bioenergy 62:108–116. https://doi.org/10.1016/j.biombioe.2014.01.008

Hoffmann H, Nieto H, Jensen R et al (2015) Estimating evapotranspiration with thermal UAV data and two source energy balance models. Hydrol Earth Syst Sci Discuss 12:7469–7502. https://doi.org/10.5194/hessd-12-7469-2015

Huang J, Ma H, Su W et al (2015) Jointly Assimilating MODIS LAI and ET Products Into the SWAP Model for Winter Wheat Yield Estimation. IEEE J Select Top Appl Earth Observ Remote Sens 8:4060–4071. https://doi.org/10.1109/JSTARS.2015.2403135

Huete A, Didan K, Miura T et al (2002) Overview of the radiometric and biophysical performance of the MODIS vegetation indices. Remote Sens Environ 83:195–213. https://doi.org/10.1016/S0034-4257(02)00096-2

Jackson RD, Hatfield JL, Reginato RJ et al (1983) Estimation of daily evapotranspiration from one time-of-day measurements. Agric Water Manag 7:351–362. https://doi.org/10.1016/0378-3774(83)90095-1

Jofre-Čekalović C, Nieto H, Girona J et al (2022) Accounting for almond crop water use under different irrigation regimes with a two-source energy balance model and copernicus-based inputs. Remote Sens 14:2106. https://doi.org/10.3390/rs14092106

Kalita PK, Kanwar RS (1992) Energy balance concept in the evaluation of water table management effects on corn growth: experimental investigation. Water Resour Res 28:2753–2764. https://doi.org/10.1029/92wr01430

Kelly J, Kljun N, Olsson P-O et al (2019) Challenges and best practices for deriving temperature data from an uncalibrated UAV thermal infrared camera. Remote Sens 11:567. https://doi.org/10.3390/rs11050567

Khan MS, Baik J, Choi M (2021) A physical-based two-source evapotranspiration model with Monin-Obukhov similarity theory. Gisci Remote Sens 58:88–119. https://doi.org/10.1080/15481603.2020.1857625

Khosa FV, Feig GT, van der Merwe MR et al (2019) Evaluation of modeled actual evapotranspiration estimates from a land surface, empirical and satellite-based models using in situ observations from a South African semi-arid savanna ecosystem. Agric for Meteorol 279:107706. https://doi.org/10.1016/j.agrformet.2019.107706

Knipper KR, Kustas WP, Anderson MC et al (2019) Evapotranspiration estimates derived using thermal-based satellite remote sensing and data fusion for irrigation management in California

vineyards. Irrig Sci 37:431–449. https://doi.org/10.1007/s00271-018-0591-y
Köksal ES, Cemek B, Artik C, Temizel KE, Taşan M (2011) A new approach for neutron moisture meter calibration: artificial neural network. Irrig Sci 29(2011):369–377. https://doi.org/10.1007/s00271-010-0246-0
Köksal ES, Tasan M, Artik C, Gowda P (2017) Evaluation of financial efficiency of drip-irrigation of red pepper based on evapotranspiration calculated using an iterative soil water-budget approach. Sci Hortic 226:398–405. https://doi.org/10.1016/j.scienta.2017.08.025
Köksal ES, Artik C, Tasan M (2018) Crop evapotranspiration estimations of red pepper using field level remote sensing data and energy balance. Pol J Environ Stud 28:165–175. https://doi.org/10.15244/pjoes/85351
Küçüktopcu E, Cemek B, Simsek H (2022) Application of spatial analysis to determine the effect of insulation thickness on energy efficiency and cost savings for cold storage. Processes 10:2393. https://doi.org/10.3390/pr10112393
Kustas WP, Norman JM (1999) Evaluation of soil and vegetation heat flux predictions using a simple two-source model with radiometric temperatures for partial canopy cover. Agric for Meteorol 94:13–29. https://doi.org/10.1016/S0168-1923(99)00005-2
Lamm FR, AbouKheira AA, Trooien TP (2010) Sunflower, soybean, and grain sorghum crop production as affected by dripline depth. Appl Eng Agric 26:873–882. https://doi.org/10.13031/2013.34952
Li Y, Huang C, Hou J et al (2017) Mapping daily evapotranspiration based on spatiotemporal fusion of ASTER and MODIS images over irrigated agricultural areas in the Heihe River Basin, Northwest China. Agric for Meteorol 244–245:82–97. https://doi.org/10.1016/j.agrformet.2017.05.023
Li C, Li Z, Gao Z, Sun B (2021) Estimation of evapotranspiration in sparse vegetation areas by applying an optimized two-source model. Remote Sens 13:1344. https://doi.org/10.3390/rs13071344
Liang W-Z, Possignolo I, Qiao X et al (2021) Utilizing digital image processing and two-source energy balance model for the estimation of evapotranspiration of dry edible beans in western Nebraska. Irrig Sci 39:617–631. https://doi.org/10.1007/s00271-021-00721-7
Liaqat UW, Choi M (2015) Surface energy fluxes in the Northeast Asia ecosystem: SEBS and METRIC models using landsat satellite images. Agric for Meteorol 214–215:60–79. https://doi.org/10.1016/j.agrformet.2015.08.245
Long D, Singh VP (2012) A Two-source Trapezoid Model for Evapotranspiration (TTME) from satellite imagery. Remote Sens Environ 121:370–388. https://doi.org/10.1016/j.rse.2012.02.015
Malbéteau Y, Parkes S, Aragon B et al (2018) Capturing the diurnal cycle of land surface temperature using an unmanned aerial vehicle. Remote Sens 10:1407. https://doi.org/10.3390/rs10091407
Mecikalski JR, Diak GR, Anderson MC, Norman JM (1999) Estimating fluxes on continental scales using remotely sensed data in an atmospheric–land exchange model. J Appl Meteorol Climatol 38:1352–1369. https://doi.org/10.1175/1520-0450(1999)038%3c1352:EFOCSU%3e2.0.CO;2
Meier F, Scherer D, Richters J et al (2011) Atmospheric correction of thermal-infrared imagery of the 3-D urban environment acquired in oblique viewing geometry. Atmosp Meas Techn 4(5):909–922. https://doi.org/10.5194/amt-4-909-2011
Mesas-Carrascosa FJ, Pérez-Porras F, Meroño de Larriva JE et al (2018) Drift correction of lightweight microbolometer thermal sensors on-board unmanned aerial vehicles. Remote Sens-Basel 10:615. https://doi.org/10.3390/rs10040615
Mokhtari A, Noory H, Pourshakouri F et al (2019) Calculating potential evapotranspiration and single crop coefficient based on energy balance equation using Landsat 8 and Sentinel-2. ISPRS J Photogramm Remote Sens 154:231–245. https://doi.org/10.1016/j.isprsjprs.2019.06.011
Mokhtari A, Ahmadi A, Daccache A, Drechsler K (2021) Actual evapotranspiration from UAV images: a multi-sensor data fusion approach. Remote Sens 13:2315. https://doi.org/10.3390/rs13122315
Moorhead JE, Marek GW, Colaizzi PD et al (2017) Evaluation of sensible heat flux and evapotranspiration estimates using a surface layer scintillometer and a large weighing lysimeter. Sensors. https://doi.org/10.3390/s17102350
Morillas L, Villagarcía L, Domingo F et al (2014) Environmental factors affecting the accuracy of surface fluxes from a two-source model in Mediterranean drylands: upscaling instantaneous to daytime estimates. Agric for Meteorol 189–190:140–158. https://doi.org/10.1016/j.agrformet.2014.01.018
Mutanga O, Skidmore AK (2004) Narrow band vegetation indices overcome the saturation problem in biomass estimation. Int J Remote Sens 25:3999–4014. https://doi.org/10.1080/01431160310001654923
Nassar A, Torres-Rua A, Kustas W et al (2021) Assessing daily evapotranspiration methodologies from one-time-of-day sUAS and EC information in the GRAPEX project. Remote Sens (Basel) 13:2887. https://doi.org/10.3390/rs13152887
Nassar A, Torres-Rua A, Hipps L et al (2022) Using remote sensing to estimate scales of spatial heterogeneity to analyze evapotranspiration modeling in a natural ecosystem. Remote Sens 14:372. https://doi.org/10.3390/rs14020372
Norman JM, Kustas WP, Humes KS (1995) Source approach for estimating soil and vegetation energy fluxes in observations of directional radiometric surface temperature. Agric for Meteorol 77:263–293. https://doi.org/10.1016/0168-1923(95)02265-Y
Norman JM, Kustas WP, Prueger JH, Diak GR (2000) Surface flux estimation using radiometric temperature: a dual-temperature-difference method to minimize measurement errors. Water Resour Res 36:2263–2274. https://doi.org/10.1029/2000wr900033
Olbrycht R, Więcek B, De Mey G (2012) Thermal drift compensation method for microbolometer thermal cameras. Appl Opt 51(11):1788–1794. https://doi.org/10.1364/AO.51.001788
Peng J, Nieto H, Andersen MN et al (2023) Accurate estimates of land surface energy fluxes and irrigation requirements from UAV-based thermal and multispectral sensors. ISPRS J Photogramm Remote Sens 198:238–254. https://doi.org/10.1016/j.isprsjprs.2023.03.009
Phasinam K, Kassanuk T, Shinde PP et al (2022) Application of IoT and cloud computing in automation of agriculture irrigation. J Food Qual. https://doi.org/10.1155/2022/8285969
Potgieter AB, George-Jaeggli B, Chapman SC et al (2017) Multi-spectral imaging from an unmanned aerial vehicle enables the assessment of seasonal leaf area dynamics of sorghum breeding lines. Front Plant Sci 8:1532. https://doi.org/10.3389/fpls.2017.01532
Sakellariou-Makrantonaki M, Papalexis D, Nakos N, Kalavrouziotis IK (2007) Effect of modern irrigation methods on growth and energy production of sweet sorghum (var. Keller) on a dry year in Central Greece. Agric Water Manag 90:181–189. https://doi.org/10.1016/j.agwat.2007.03.004
Sánchez JM, Kustas WP, Caselles V, Anderson MC (2008) Modelling surface energy fluxes over maize using a two-source patch model and radiometric soil and canopy temperature observations. Remote Sens Environ 112:1130–1143. https://doi.org/10.1016/j.rse.2007.07.018
Sánchez JM, López-Urrea R, Rubio E, Caselles V (2011) Determining water use of sorghum from two-source energy balance and radiometric temperatures. Hydrol Earth Syst Sci 15:3061–3070. https://doi.org/10.5194/hess-15-3061-2011
Sánchez JM, López-Urrea R, Rubio E et al (2014) Assessing crop coefficients of sunflower and canola using two-source energy balance

and thermal radiometry. Agric Water Manag 137:23–29. https://doi.org/10.1016/j.agwat.2014.02.002
Sánchez JM, López-Urrea R, Doña C et al (2015) Modeling evapotranspiration in a spring wheat from thermal radiometry: crop coefficients and E/T partitioning. Irrig Sci 33:399–410. https://doi.org/10.1007/s00271-015-0476-2
Sau F, Boote KJ, McNair Bostick W et al (2004) Testing and improving evapotranspiration and soil water balance of the DSSAT crop models. Agron J 96:1243–1257. https://doi.org/10.2134/agronj2004.1243
Senay GB, Budde M, Verdin JP, Melesse AM (2007) A coupled remote sensing and simplified surface energy balance approach to estimate actual evapotranspiration from irrigated fields. Sensors 7:979–1000. https://doi.org/10.3390/s7060979
Senay GB, Bohms S, Singh RK et al (2013) Operational evapotranspiration mapping using remote sensing and weather datasets: a new parameterization for the SSEB approach. J Am Water Resour Assoc 49:577–591. https://doi.org/10.1111/jawr.12057
Shafian S, Rajan N, Schnell R et al (2018) Unmanned aerial systems-based remote sensing for monitoring sorghum growth and development. PLoS ONE 13:e0196605. https://doi.org/10.1371/journal.pone.0196605
Simpson JE, Holman F, Nieto H et al (2021) High spatial and temporal resolution energy flux mapping of different land covers using an off-the-shelf unmanned aerial system. Remote Sens 13:1286. https://doi.org/10.3390/rs13071286
Singh RK, Ayse I, Suat I, Martin DL (2008) Application of SEBAL model for mapping evapotranspiration and estimating surface energy fluxes in South-Central Nebraska. J Irrig Drain Eng 134:273–285. https://doi.org/10.1061/(ASCE)0733-9437(2008)134:3(273)
Song B, Park K (2020) Verification of accuracy of unmanned aerial vehicle (UAV) land surface temperature images using in-situ data. Remote Sens 12:288. https://doi.org/10.3390/rs12020288
Song L, Kustas WP, Liu S et al (2016) Applications of a thermal-based two-source energy balance model using Priestley-Taylor approach for surface temperature partitioning under advective conditions. J Hydrol 540:574–587. https://doi.org/10.1016/j.jhydrol.2016.06.034
Taheri M, Mohammadian A, Ganji F et al (2022) Energy-based approaches in estimating actual evapotranspiration focusing on land surface temperature: a review of methods, concepts, and challenges. Energies 15:1264. https://doi.org/10.3390/en15041264
Tang R, Li Z-L, Tang B (2010) An application of the Ts–VI triangle method with enhanced edges determination for evapotranspiration estimation from MODIS data in arid and semi-arid regions: Implementation and validation. Remote Sens Environ 114:540–551. https://doi.org/10.1016/j.rse.2009.10.012
Todd RW, Evett SR, Howell TA (2000) The Bowen ratio-energy balance method for estimating latent heat flux of irrigated alfalfa evaluated in a semi-arid, advective environment. Agric for Meteorol 103:335–348. https://doi.org/10.1016/S0168-1923(00)00139-8
Togneri R, Kamienski C, Dantas R et al (2019) Advancing IoT-based smart irrigation. IEEE Internet of Things Mag 2:20–25. https://doi.org/10.1109/IOTM.0001.1900046
Tunca E, Köksal ES, Çetin S et al (2018) Yield and leaf area index estimations for sunflower plants using unmanned aerial vehicle images. Environ Monit Assess 190:682. https://doi.org/10.1007/s10661-018-7064-x
Tunca E, Köksal ES, Torres-Rua AF et al (2022) Estimation of bell pepper evapotranspiration using two-source energy balance model based on high-resolution thermal and visible imagery from unmanned aerial vehicles. JARS 16:022204. https://doi.org/10.1117/1.JRS.16.022204
Vinukollu RK, Meynadier R, Sheffield J, Wood EF (2011) Multi-model, multi-sensor estimates of global evapotranspiration: climatology, uncertainties and trends. Hydrol Process 25:3993–4010. https://doi.org/10.1002/hyp.8393
Wandera L, Mallick K, Kiely G et al (2017) Upscaling instantaneous to daily evapotranspiration using modelled daily shortwave radiation for remote sensing applications: an artificial neural network approach. Hydrol Earth Syst Sci 21:197–215. https://doi.org/10.5194/hess-21-197-2017
Zhuang Q, Wu B (2015) Estimating evapotranspiration from an improved two-source energy balance model using ASTER satellite imagery. Water 7:6673–6688. https://doi.org/10.3390/w7126653
Zou Y, Saddique Q, Ali A et al (2021) Deficit irrigation improves maize yield and water use efficiency in a semi-arid environment. Agric Water Manag 243:106483. https://doi.org/10.1016/j.agwat.2020.106483